Poly(propylene)/Graphene Nanoplatelet Nanocomposites: Melt Rheological Behavior and Thermal, Electrical, and Electronic Properties

Yunfeng Li, Jiahua Zhu, Suying Wei, Jongeun Ryu, Luyi Sun, Zhanhu Guo*

Poly(propylene) polymer nanocomposites containing graphene nanoplatelets (GnPs) with different loadings are fabricated via a facile ex-situ solution approach. Improved thermal stability and higher crystallinity are observed in the PNCs. Both electrical conductivity and real permittivity increase with increasing GnP loading. Electrical conductivity percolation is observed at 12.0 wt% GnP. The rheological behavior of the PNC melts are also investigated. It is found that the modulus and viscosity are reduced at small GnP loadings and increased above a critical loading.

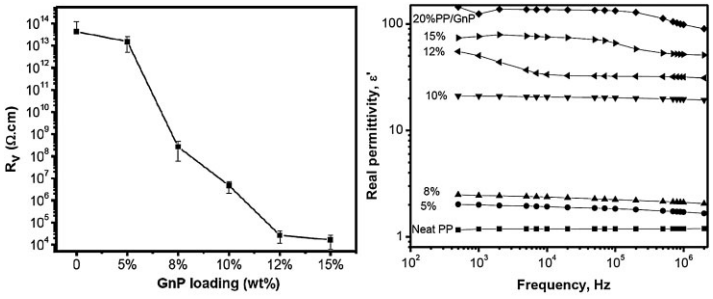

Introduction

Modification of polymers by adding nanofillers as a second phase has become a practical strategy to improve the parent polymer material properties such as stiffness, thermal stability, and electrical conductivity[1–10] and to introduce unique physical properties such as magnetic, optical, and electrochromic properties.[11–14] A wide range of thermoplastics, including poly(propylene) (PP),[15–19] polyethylene,[20–22] poly(methyl methacrylate),[23] polystyrene,[24–27] and polycarbonate[28] have been reinforced with layered silicates and carbon materials such as carbon nanotubes (CNTs), carbon blacks and vapor-grown carbon nanofibers (VGCNFs). PP is one of the most widely used commodity thermoplastics with a very simple chemical structure. These PP nanocomposites containing carbon materials of less than 100 nm at least in one dimension are considered for many applications, including interior and exterior parts of automobiles, structural materials for electronic devices, and fuel cells.[25,29–34]

Graphene nanoplatelets (GnPs), also named exfoliated graphite nanoplatelets, combining the layer structure and low cost with excellent thermal, electrical, and mechanical properties, compete with carbon nanofibers (CNFs) and CNTs for the preparation of polymer nanocomposites (PNCs).[16,35,36] Graphite is the stiffest material found in nature with a Young's Modulus of almost 1 TPa,[37,38] which is several times higher than that of clay, and also possess

Y. Li, J. Zhu, Z. Guo
Integrated Composites Laboratory (ICL), Dan F. Smith Department of Chemical Engineering, Lamar University, Beaumont, TX 77710, USA
E-mail: zhanhu.guo@lamar.edu
Y. Li, S. Wei
Department of Chemistry and Biochemistry, Lamar University, Beaumont, TX 77710, USA
J. Ryu
Department of Mechanical & Aerospace Engineering, University of California Los Angeles, Los Angeles, CA 90095, USA
L. Sun
Department of Chemistry and Biochemistry, Texas State University-San Marcos, San Macros, TX 78666, USA

DOI: 10.1002/macp.201100263

excellent strength, electrical, and thermal conductivity ($\approx 5 \times 10^3$ $W \cdot m^{-1} \cdot K^{-1}$).[39,40] Since graphite intercalation compounds (GICs) based on natural crystalline graphite are quite cheap, around \$1.5–1.6/lb,[36] the cost of exfoliated graphite nanoplatelets is expected to be \$5/lb or less.[36] This is significantly less expensive than CNTs ($\approx$\$100 g^{-1}) or VGCNFs (\$40–50/lb),[39] the properties of crystalline graphite nanoplatelets are comparable to those of the CNTs and VGCNFs. With an appropriate and practical method to disperse the GnPs in the polymer matrix, the PNCs will possess excellent thermal and electrical conductivity and outstanding mechanical properties, which will have many potential applications where electromagnetic shielding and high electrical and thermal conductivity are required. With the incorporation of CNFs to the polymeric matrix, an improved thermal stability and flame retardancy have been reported, which could serve as an alternative to the conventional flame retardants.[16,17,39] The formed carbon nanofiller network structure increases the heat transfer to the surrounding and thus retard the flame.[41,42] Meanwhile, a sharp increased electric conductivity (σ) is observed in the PNCs and this corresponding filler loading is normally defined as percolation threshold (P_c) with a continuous conductive network formed in the insulating polymer matrix.[16,17,39] The melt rheological property provides a convenient way to evaluate the dispersion state of the nanofillers in the polymer matrix.[16,43,44] It is feasible to monitor the microstructural evolution by using some rheological parameters such as storage modulus and viscosity as indicators.[44] The change from a liquid-like to a pseudo-solid-like flow behavior was observed in the PNCs with the nanofiller loading above a critical value, at which the σ and dielectric property will change dramatically.[1,2,16,43] Thus, the melt rheological results can also provide filler distribution information in the topic of PP/GnP PNCs. To correlate the percolation values obtained from σ, dielectric permittivity and rheology is not a trivial for the obtained economical and useful PP/GnP PNCs, which have not been systematically investigated yet.

In this paper, PP/GnP PNCs with various GnP loadings are fabricated using a facile solvent dispersion strategy. The effects of the incorporated GnPs on the thermal stability, crystallinity and rheological behavior of PP are investigated. Electrical conductivity and dielectric properties of the PP/GnP nanocomposites are discussed as well.

Experimental Section

Materials

The isotactic PP used in this study was supplied by Total Petrochemicals USA, Inc ($\rho = 0.9\ g \cdot cm^{-3}$, $\overline{M}_n \approx 40\,500$, $\overline{M}_w \approx 155\,000$, melt index: $\approx 35\ g \cdot min^{-1}$). GnPs were produced by Angstron Materials, Inc. and used as received. The products are designated as N008-100-P-40. The thickness of the platelets (Z direction) is 50–100 nm and the average length (X and Y direction) is in the range of 40–50 μm. The solvent xylene (XX0060-3, maximum residue after evaporation: 0.002%, maximum amount of water: 0.05%) with a boiling temperature ranging from 137 to 145 °C was obtained from EM Industries, Inc.

Preparation of PP/GnP Nanocomposites

PP and xylene were charged into a beaker. The weight ratio of PP and xylene is 1:10, and the content of GnP in the final composites are 0, 5.0, 10.0, 15.0, and 20.0 wt%, respectively. The corresponding volume concentrations were 0, 2.11, 4.35, 6.73, and 9.28 vol%. The GnP volume content can be determined from the GnP density (ca. 2.2 $g \cdot cm^{-3}$) and PP.[17]

The PP/xylene mixture was heated and stirred with a magnetic bar to around 70 °C for 2 h. A transparent viscous solution was observed after PP dissolved completely in xylene. The viscous solution was mixed with a predetermined amount of GnPs, then the above heating and stirring process was repeated overnight. However, the agglomeration of GnPs would form if the stirring stops. Thus, the mixture was immediately added into the low-temperature deionized water to extract solidify the PNCs by extracting xylene with water right after the heating process was finished. Afterwards, the solidified organic phase system was evaporated at room temperature in the fume hood for 48 h to eliminate xylene. The resulting PP/GnP PNCs were used to make discs with a 25 mm diameter on the hot-press machine (Carver 3853-0, USA). Briefly, the dried powders were compressed under a pressure of 10 MPa at 180 °C in a mold at a heating rate of 20 °C $\cdot$ min^{-1}. The compressed composites were held at 180 °C for 20 min and then cooled down to room temperature in the mold while maintaining the applied pressure. Finally, a disk-shaped PNC sample was prepared with a diameter of 25 mm and thickness of 2–3 mm. These discs were stored in a vacuum chamber for further studies. Figure 1 depicts the main experimental set-ups and the procedures for the nanocomposite preparation.

Characterizations

The powder X-ray diffraction (XRD) analysis of the samples was carried out with a Bruker AXS D8 Discover diffractometer with GADDS (General Area Detector Diffraction System) operating with a Cu K_α radiation source filtered with a graphite monochromator ($\lambda = 1.5406$ Å). The detector used was a HI-STAR two-dimensional multi-wire area detector. The samples were loaded onto double sided scotch tape, placed on a glass slide, and mounted on a quarter-circle Eulerian cradle (Huber) on an XYZ stage. The X-ray beam was generated at 40 kV and 40 mA power and was collimated to about an 800-mm spot size on the sample. The incident ω angle was 5°. A laser video system was used to ensure the alignment of the sample position on the instrument center. XRD scans were recorded from $2\theta = 7$ to 77° with a 0.050° step width and 60 s counting time for each step. The XRD data were analyzed using the DIFFRAC-Plus EVA program (Bruker AXS, Karlsruhe, Germany), and the patterns were identified using the ICDD PDFMaint computer reference database.

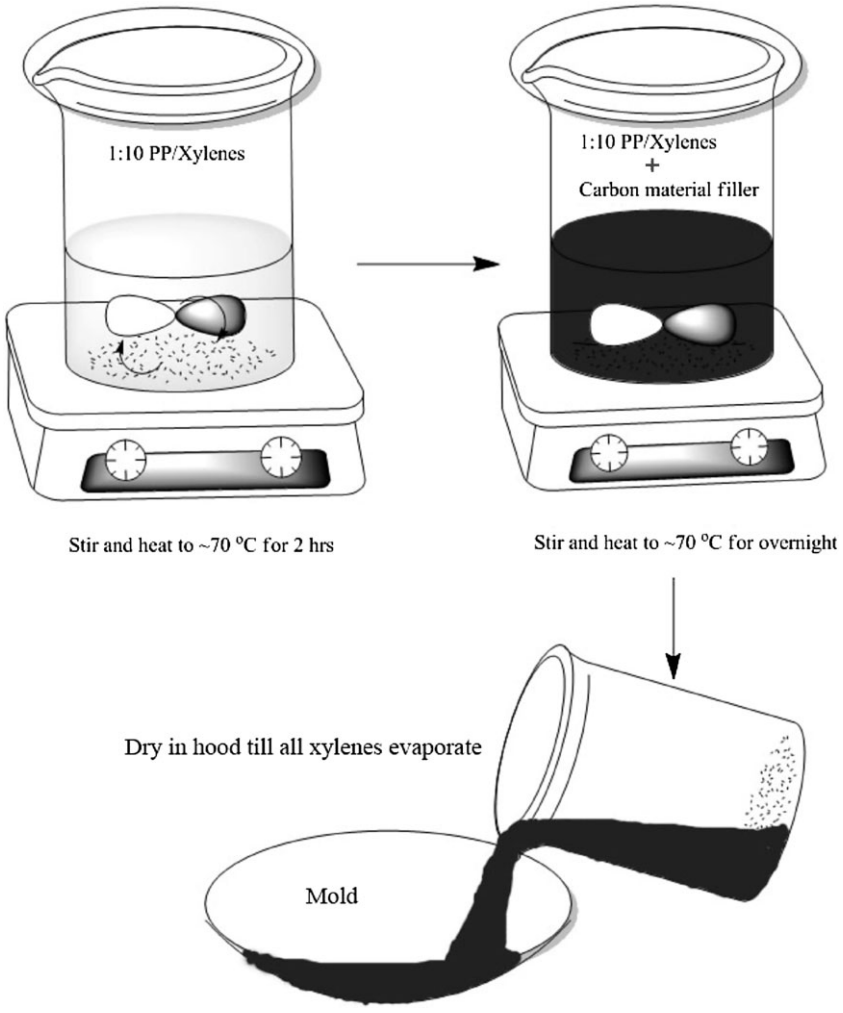

Figure 1. Experimental setup and the procedure for nanocomposites preparation.

The morphology and microstructure of the neat PP and its GnP PNCs was studied using scanning electron microscopy (SEM, JEOL field emission scanning electron microscope, JSM-6700F). All disc samples were dipped into liquid nitrogen and fractured. The fractured surfaces were sputter-coated to prevent changing and to improve image quality.

In order to study the thermal stability and crystallization behavior of the neat PP and PP/GnP PNCs, both thermogravimetric analysis (TGA) and differential scanning calorimetry (DSC) were employed. The TGA experiments were carried out using a TA Instruments Q500 analyzer under a heating rate 10 °C · min^{-1} and an air flow rate of 60 mL · min^{-1} from 25 to 800 °C. A TA Instruments Q2000 differential scanning calorimeter was used to obtain DSC thermograms. Experiments were run on samples of about 8–10 mg. Each sample was first heated from room temperature to 200 °C with a heating rate of 10 °C · min^{-1} to remove thermal history, followed by cooling down to 40 °C at a rate of 10 °C · min^{-1} to record re-crystallization temperature, and then reheat to 200 °C at the same rate to determine the melt temperature. The experiments were carried out under a nitrogen purge (50 mL · min^{-1}).

The volume resistance (R_v) of the samples was measured by an Agilent 4339B high resistance meter after obtaining the thickness of these composites pellets. The voltage and current limits were set at 1.0 V and 5 mA for all samples. Agilent E4980A Precision LCR Meter (20–2MHz) with signal voltage range of 0–2.0 V_{rms} and signal current range of 0–20.0 mA_{rms} was used to collect the dielectric data at room temperature. The frequency range in the measurement was 500–2 MHz.

The melt rheological behaviors of the neat PP and its GnP PNCs were studied by a TA Instruments AR 2000ex Rheometer. The frequency sweep was from 100 to 0.1 rad · s^{-1} and the temperature was 200 °C when PP was in melt state. The measurements were performed in an ETC Steel parallel plate (25 mm diameter of upper geometry) in nitrogen with 20% strain, which was checked to be in the linear viscoelastic region (i.e., stress and strain were related linearly).

Results and Discussion

Morphology

SEM observations have shown the flake like shape of the pristine GnPs and consistent with the prior observation,[45] see Figure 2. Figure 3(a–d) shows the microstructures of the PP/GnP PNCs with a GnP loading of 5.0 and 15.0 wt%, respectively. Note that the SEM images were taken on the fractured surfaces by dipping the samples into liquid nitrogen and then breaking them by a hammer. As

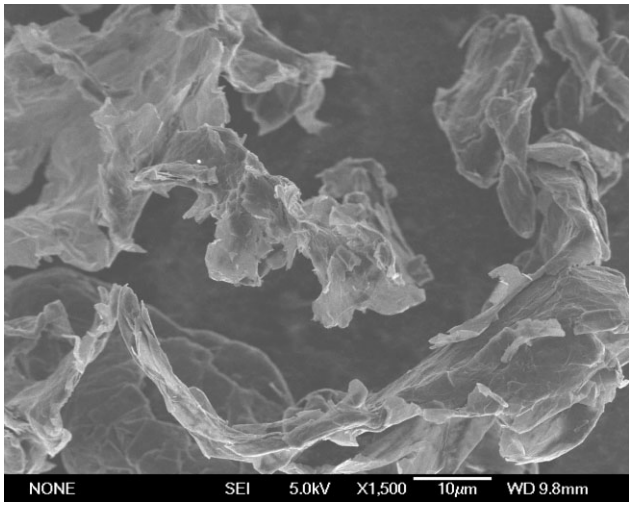

Figure 2. SEM image of the pristine GnPs.

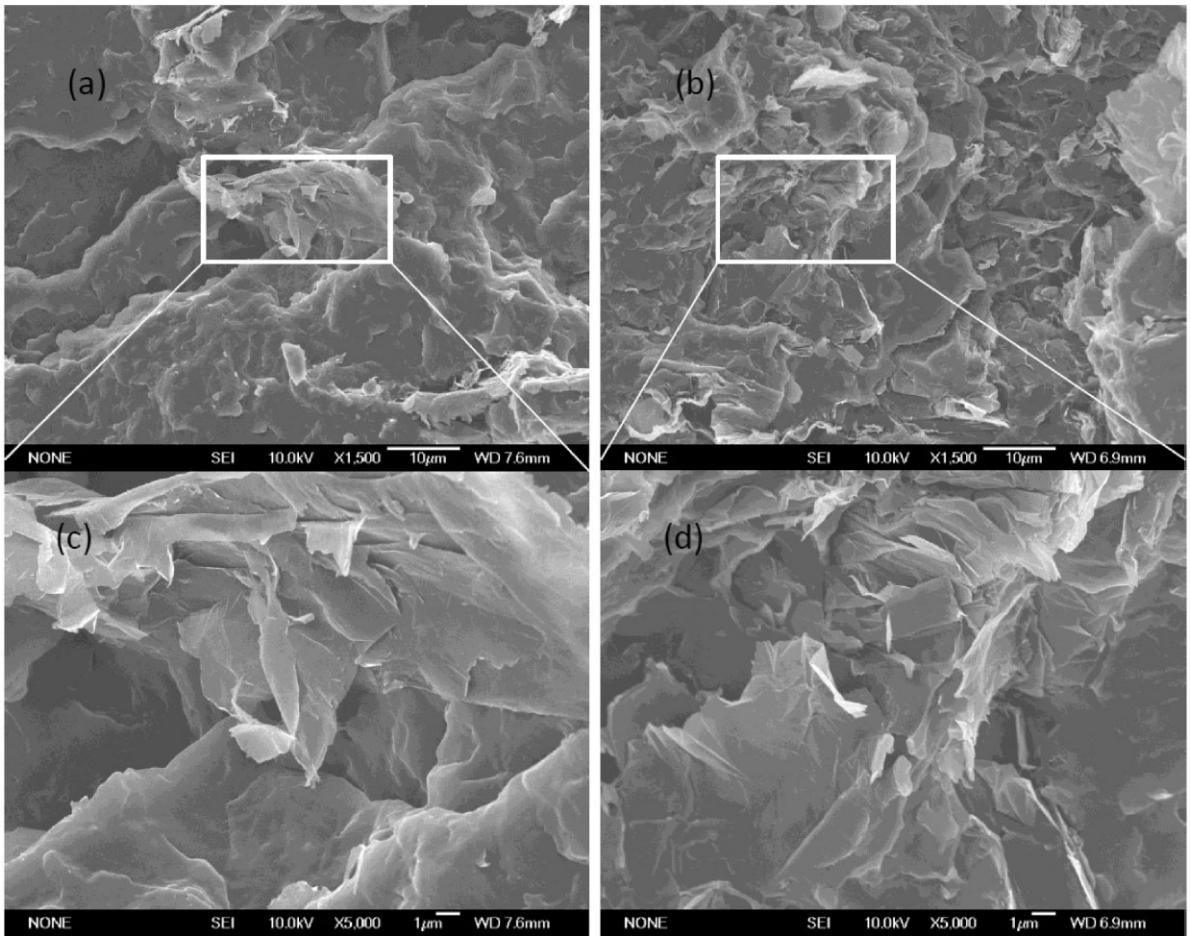

Figure 3. SEM images of the PP PNCs with a graphene nanoplatelets loading of (a) 5.0 and (b) 15.0 wt%. Parts (c) and (d) are the enlarged (a) and (b), respectively.

shown in Figure 3(a), the GnPs are separated from each other in the PNCs with a GnP loading of 5.0 wt%. When the GnP loading increases, the GnPs are observed to be close to each other, which results in a dense dispersion of GnPs in the PP/GnP PNCs with a loading of 15.0 wt%, Figure 3(b). Further investigation of those high resolution SEM images, Figure 3(c and d) of the PNCs with 5.0 and 15.0 wt% GnP loading reveals the GnP agglomeration and being wrinkled when they are incorporated into the PP matrix, indicating that the layers of these GnPs are not fully utilized.

XRD

Figure 4 depicts the XRD patterns of neat PP and its GnP PNCs. The peaks at approximately 14.2, 17.0, 18.8, and 20.0° correspond to the (110), (040), (130), and (111) planes of α crystal of PP, respectively,[46,47] while the overlapping peaks between 21.1 and 22.1°, indicated by a black arrow in Figure 4, are attributed to a combination of α-phase (131 and 041) and β-phase (301) of PP.[47] The small peak at 25.4°

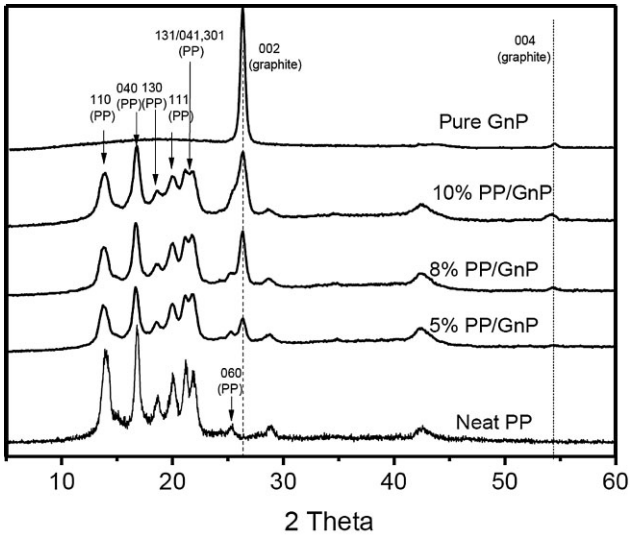

Figure 4. XRD patterns of pure PP and PP/GnP nanocomposites.

corresponds to α-form PP (060).[46] The peak at around 26.7° is the (002) plane of the exfoliated graphite nanoplatelets and the one at 54.8° corresponds to (004) of graphite.[48–50] The intensities of both peaks become stronger with increasing the filler loading. PP crystalline polymorph is barely affected by the incorporated GnPs, which is consistent with the reported results.[17]

Thermal Properties of GnP/PP Composites

Figure 5(A) shows the TGA weight loss curves of the neat PP, pure GnP, and PP/GnP PNCs, and Figure 5(B) shows the corresponding derivative weight loss curves. The normalized sample mass is slightly less than 100% after 215 °C. The GnP sample is also slightly less than 100% due to the loss of moisture and organic impurities. In the range of 360–500 °C, the pure GnP is extremely thermally stable. Noticeably, the relationship between the GnP loading and the corresponding temperature of the maximum rate of the weight loss is almost linear, the inset Figure 5(B). As the GnP loading increases, the decomposition temperatures are correspondingly elevated in the PP/GnP PNCs.

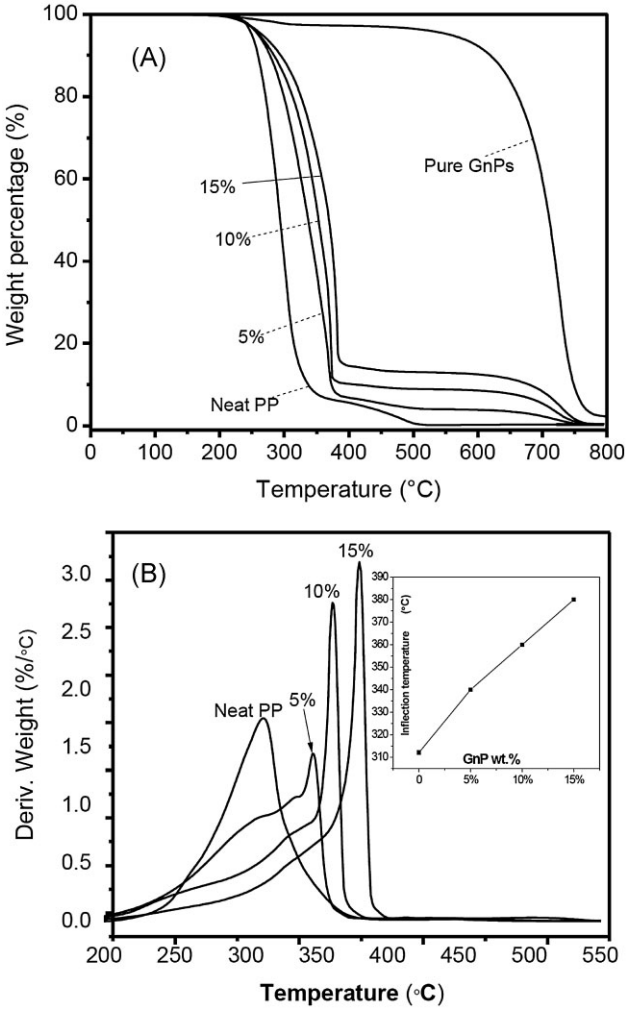

Figure 5. (A) TGA weight loss curves and (B) derivative weight loss curves of pure PP, GnPs, and PP/GnP PNCs. Inserted shows linear relationship between GnP loading and inflection point.

Table 1. TGA data of pure PP and GnP/PP nanocomposites. $T_{10\%}$: temperature of 10% mass loss; T_{max}: inflection point; T_{end}: end temperature of the degradation; T_r: degradation temperature range.

GnP loading [wt%]	$T_{10\%}$ [°C]	T_{max} [°C]	T_{end} [°C]	T_r [°C]
0	259	312	365	106
5	277	340	374	97
10	285	360	376	125
15	295	380	385	132

The 10% mass loss temperatures ($T_{10\%}$), the temperatures of the maximum weight loss rate (inflection point, T_{max}), the end temperatures of the degradation (T_{end}) and the degradation temperature ranges (T_r) are summarized in Table 1. $T_{10\%}$ and T_{max} listed in Table 1 show that the PP/GnP PNCs exhibit an improved thermal stability than that of neat PP. The enhanced thermal stability of the PP/GnP PNCs results from the interaction between PP matrix and the GnPs. The surface of the GnPs absorbs the free radicals produced in the decomposition of PP and restricts the mobility of the polymer molecules, which retards the degradation of the PP/CnP PNCs.[41,42]

Figure 6 compares the non-isothermal crystallization curves as measured by DSC. The incorporation of GnPs is

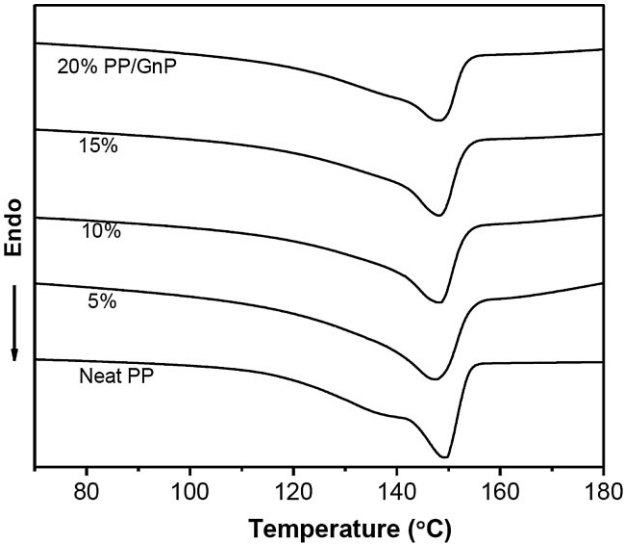

Figure 6. DSC thermograms (second heating cycle) of neat PP and GnP/PP nanocomposites.

Table 2. DSC data (second heating cycle) of neat PP and GnP/PP nanocomposites. T_{on}: onset melting temperature; T_m: melting temperature; ΔH_m: melting enthalpy; D: degree of crystallinity; ΔD: variation in the degree of crystallinity.

GnP loading [wt%]	T_{on} [°C]	T_m [°C]	H_m [J · g^{-1}]	D [%]	ΔD [%]
0	136.4	149.4	69.08	33.05	–
5	139.3	147.3	66.75	33.62	0.57
10	139.4	148.0	70.10	37.26	4.21
15	140.4	148.1	68.42	38.51	5.46
20	141.1	148.7	65.28	39.04	5.99

observed to have little effect on the melting temperature (about 149 °C) and slightly increases the onset melting temperature (T_m) compared to that of pure PP. However, an increase in the GnP loading leads to wider and shallower exothermic curves, which indicates that the dispersed GnPs act as barriers to the formation of large PP crystallites.[16] The onset melting temperature (T_{on}), melting temperature (T_m), melting enthalpy (ΔH_m), degree of crystallinity (D) and the variation in the degree of crystallinity (ΔD) are summarized and listed in Table 2. The relationship between ΔH_m and D is

$$D = \frac{\Delta H_m}{\Delta H_0 f_{PP}} \times 100\% \quad (1)$$

where ΔH_0 is the melting enthalpy of the 100% crystalline PP, which is reported to be 209 J · g^{-1},[51] and f_{PP} is the PP weight fraction in the composites. One can see from Table 2, for the composites with GnP 10 wt% or above, D is also increased 4–6% as compared to that of pure PP.

Electric Conductivity and Dielectric Properties of the PP/GnP Nanocomposites

Figure 7 shows the electrical resistivity of neat PP and its GnP PNCs. As compared with that of the pure polymer, a slight decrease in the volume resistivity is observed in the PNCs with a GnP loading of 5.0 wt% and the PNCs are still insulating. A pronounced drop in the surface resistivity is observed and the resistivity decreases approximately linearly as the GnP filler weight percentage increases from 5.0 to 12.0 wt%. However, when the filler content increases further to 15.0 wt% (6.73 vol%), the resistivity decreases a little to ≈1.6 × 10^4 Ω · cm^{-1} but almost keeps at the same level compared to that of 12%. This indicates that the electrical percolation falls between 8.0 and 12.0 wt% and that the cross-linked network structure of the naturally conductive GnPs has been formed, which is responsible for the high electrical conductivity of those samples with a GnP

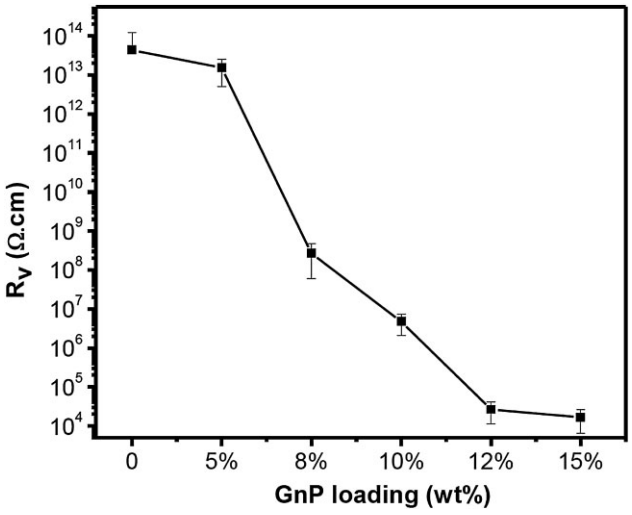

Figure 7. Volume resistivity of the PP/GnP nanocomposites as a function of GnP loading.

loading higher than 12.0 wt%. As previously shown in Figure 3, the GnPs are agglomerated and wrinkled when incorporated into the PP matrix, which explains the observed higher electrical conductivity percolation than that observed in the PP PNCs prepared by the solid-state shear pulverization method.[16] Many reports have been published regarding the electric conductivity (σ) of PP/graphite composites. It has been reported that at a filler content of 20 vol%, the volume resistivity was reduced to 10^5 Ω · cm with experimental and modeling results.[20,52] Both Keith et al.[52] and Chen et al.[20] found that σ of PP/graphite could not significantly drop when the filler content is less than 30 wt%. Typically, the σ percolation is highly influenced by the distribution of conductive fillers in the polymer matrix. A better dispersion usually leads to the formation of the cross-linked structure at a lower filler loading. As compared to the reported results, the used solvent distribution strategy here favors better filler dispersion than those reported ones.

Dielectric materials find wide applications in storing electrical energy through charge separation, which occurs when the electrons are polarized by an external electric field.[53] Since high energy storage is required in mobile electronic devices, stationary power systems, hybrid electric vehicles, and pulse power applications,[54,55] there is growing attention in the study of the dielectric property of the new materials. Here the PP/GnP PNCs have been investigated for their potential applications in the energy storage through measuring their dielectric property. The frequency dependent real permittivity (ε') of PP/GnP PNCs with various loadings at 25 °C is depicted in Figure 8. The ε' of the PP/GnP PNCs increases with increasing the filler loading in the entire frequency testing range. Similar

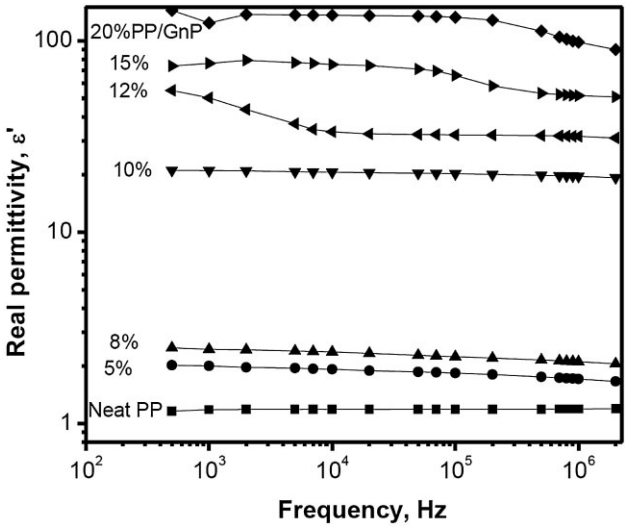

Figure 8. Real permittivity at 25 °C as a function of frequency for PP/GnP nanocomposites.

results have been reported when other carbon materials such as CNFs, were used as the filler in PP.[17] In addition, for any given GnP content, the value of ε' in PP/GnP PNCs is virtually independent of the frequency, indicating a stable dielectric performance of the prepared nanocomposites upon frequency variation.

For a parallel-plate capacitor, the capacitance is linear to its ε' of the material,[56] the magnitude of ε' also correspondingly determines the ability of a material to store energy. From Figure 8, ε' of 8.0 wt% GnP/PP composites is almost doubled that of the pure PP. As the GnP loading increases to 10.0 wt% with a formed network structure, the ε' has increased up to 100 times that of pure PP. This reveals that both σ and ε' of the PNCs sharply increase near the electrical percolation threshold. Considering that the σ saturates at 12.0 wt%, this is very close to the big jump of ε' at around 10.0 wt%, Figure 8. Compared with the ceramic counterparts, the polymer capacitors have higher breakdown voltage and better processibility.[53] Therefore, the PP/GnP PNCs with a low GnP loading and much superior dielectric performance would be promising in energy storage applications.

Rheological Behavior of PP/GnP Nanocomposite Melts

The rheological behavior of the polymer nanocomposite melts are mostly orientated to better understand the dynamics of the nanoconfined polymers. The storage and loss moduli of pure PP and its nanocomposite melts with GnP filler loading from 5.0 to 20.0 wt% at 200 °C are presented in Figure 9(A and B), with a log-log plot as a function of angular frequency (ω). The storage modulus (G') of the PNC melts increases with increasing the GnP loading, especially at low angular frequency. However, compared to the G' of pristine PP at low ω, the ones at 5.0 and 10.0 wt% GnP loading are even lower, which results from the GnP/PP interlayer slipperiness due to a low surface friction and agglomeration of GnPs. And the PNC melts behave like a viscous PP liquid.[57] After the GnP content is above the critical percolation percentage of ca. 15.0 wt%, the rheological response changes and the elastic solid-like behavior is observed, with only a limited reduction in G' at low ω. Like σ, melt-state shear storage modulus (G') is a property that is highly sensitive to the formation a network-like structure in the PNCs.

Figure 10 shows the mechanical loss factor (tan δ) as a function of ω. The tan δ, which is the ratio of loss modulus to storage modulus, is highly related to the applied ω. When scanning the experimental ω from low to high, the tan δ of

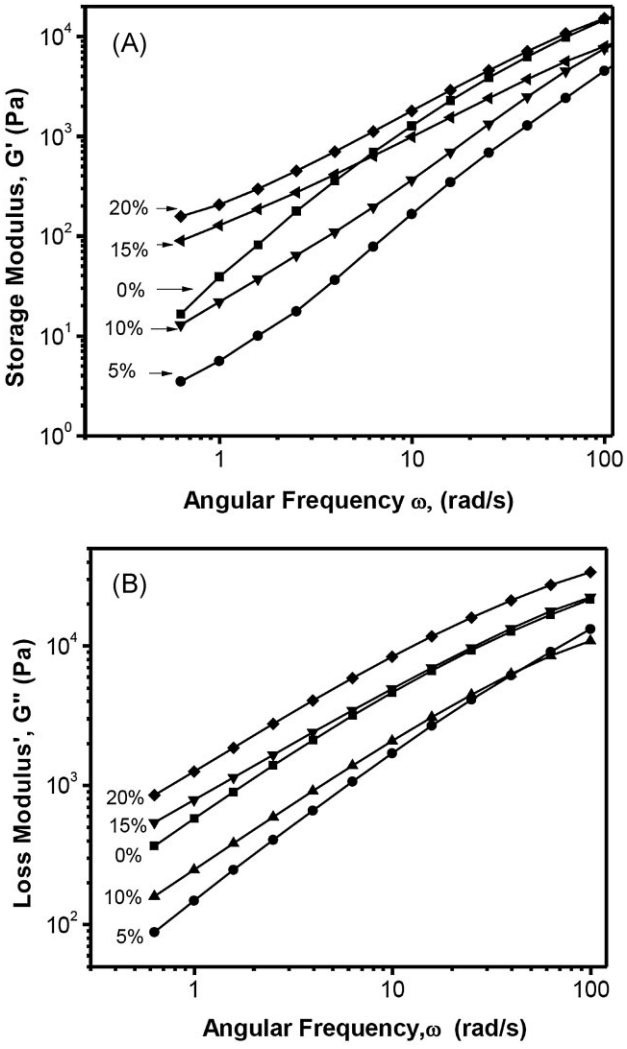

Figure 9. Plot of (A) storage modulus (G') and (B) loss modulus (G'') versus angular frequency (ω) for neat PP and its GnP nanocomposites.

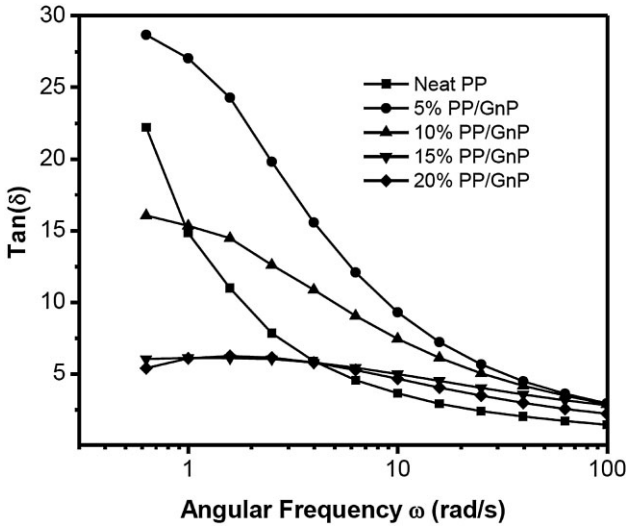

Figure 10. Mechanical loss factor (tan δ) of PP/GnP nanocomposites with different GnP loading.

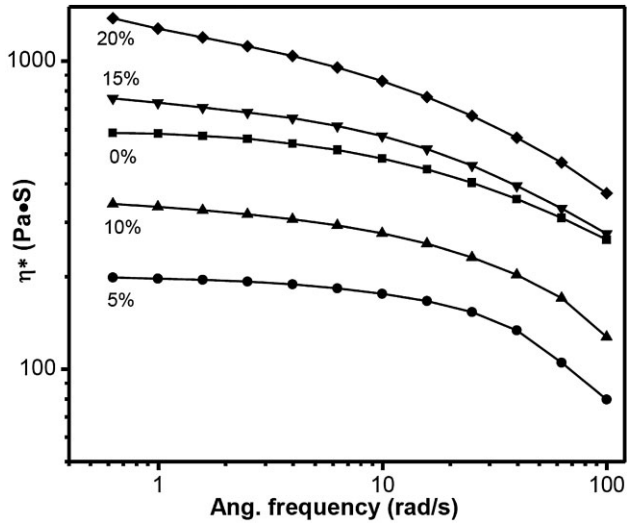

Figure 11. Complex viscosity (η^*) versus ω for pure PP and its GnP nanocomposites.

the PNC melts shows three different stages: rubbery, viscoelastic and glassy state.[17] The tan δ at rubbery and glassy state is relatively small compare to the viscoelastic state. From Figure 10, pure PP and its GnP PNCs with 5.0 and 10.0 wt% show viscoelastic state near 0.4 rad $\cdot$ s^{-1} and glass state around 100 rad $\cdot$ s^{-1}, at which their tan δ changes significantly. As from the G' plot in Figure 9, the PNCs with a 5.0 wt% GnP loading have lower G' than that of pure PP due to the slippage between GnPs. Correspondingly, it has larger tan δ. As the GnP loading increases over the percolation threshold, tan δ decreases. For GnP/PP PNCs with a loading of 15.0 and 20.0 wt%, tan δ changes much less and the tan δ peak is delayed. Thus, the rheological data agree well with the electrical resistivity data, indicating a percolation threshold in the PNCs around 10–15 wt% GnPs.

The viscosity of pure and its GnP PNC melts are also illustrated in a log-log plot of the viscosity as a function of ω, shown in Figure 11. A horizontal line indicates a Newtonian fluid and the decreased viscosity with increasing the shear rate or ω is defined as shear thinning.[33,58] Figure 11 shows the complex viscosity (η^*) of neat PP and its GnP PNC melt. η^* is observed to decrease with increasing ω, indicating that neat PP and its GnP PNCs exhibit a typical shear-thinning behavior. η^* of these PNC melts increases correspondingly with increasing the GnP loading from 5.0 to 20.0%), Figure 11. The increment of the melt viscosity results from the stronger interaction between GnP and PP matrix as the GnP filler content increases, which restricts the PP chain movements more significantly. Many other nano-carbon fillers such as CNFs, have also been reported to be able to interact strongly with the polymer matrix and cause an elevated η^*.[17] However, compared to that of pure PP, the PNCs with a loading of 5.0 and 10.0 has less η^*, which is 580 Pa $\cdot$ s at 1 rad $\cdot$ s^{-1}.

Conclusion

GnP-filled PP nanocomposites were prepared through a facile solution dispersion method. The dispersion and morphology of the GnPs in the PP matrix was investigated by SEM. The images show that the GnPs are bended and slightly aggregated in the polymer matrix. The GnP network formed at the filler loading of around 12.0 wt% was verified by the volume resistivity and dielectric property measurements. As compared to neat PP, the GnP-filled PP PNCs exhibit an improved thermal stability. The rheological behaviors were also investigated with a reduced storage modulus and complex viscosity in the PNC melts with the loading below the critical percolation threshold, and an enhanced storage modulus and complex viscosity in the PNC melts with the loading above the critical percolation threshold. The rheological results also verified that the critical percentage of GnP network formation is around 12.0 wt%.

Acknowledgements: The authors gratefully thank Dr. J. A. Gomes for assistance with XRD. This project is supported by the National Science Foundation, the Nanoscale Interdisciplinary Research Team, and Materials Processing and Manufacturing (CMMI 10-30755).

Received: May 4, 2011; Published online: July 22, 2011; DOI: 10.1002/macp.201100263

Keywords: electrical conductivity; graphene nanoplatelets; melt rheological behavior; poly(propylene)

[1] H. Kim, Y. Miura, C. W. Macosko, *Chem. Mater.* **2010**, *22*, 3441.
[2] H. Kim, A. A. Abdala, C. W. Macosko, *Macromolecules* **2010**, *43*, 6515.
[3] X. Zhang, L. S. Loo, *Macromolecules* **2009**, *42*, 5196.

[4] Y. Rao, J. M. Pochan, *Macromolecules* **2006**, *40*, 290.
[5] M. Moniruzzaman, K. I. Winey, *Macromolecules* **2006**, *39*, 5194.
[6] D. D. L. Chung, *Carbon* **2001**, *39*, 1119.
[7] S. Zhang, A. R. Horrocks, *Prog. Polym. Sci.* **2003**, *28*, 1517.
[8] J. Zhu, S. Wei, A. Yadav, Z. Guo, *Polymer* **2010**, *51*, 2643.
[9] P. Mavinakuli, S. Wei, Q. Wang, A. B. Karki, S. Dhage, Z. Wang, D. P. Young, Z. Guo, *J. Phys. Chem. C* **2010**, *114*, 3874.
[10] J. Zhu, S. Wei, J. Ryu, M. Budhathoki, G. Liang, Z. Guo, *J. Mater. Chem.* **2010**, *20*, 4937.
[11] Z. Guo, S. Park, H. T. Hahn, S. Wei, M. Moldovan, A. B. Karki, D. P. Young, *Appl. Phys. Lett.* **2007**, *90*, 053111.
[12] Z. Guo, H. Lin, A. B. Karki, D. P. Young, H. T. Hahn, *Compos. Sci. Technol.* **2008**, *68*, 2551.
[13] J. Zhu, S. Wei, M. J. Alexander, T. D. Dang, T. C. Ho, Z. Guo, *Adv. Funct. Mater.* **2010**, *20*, 3076.
[14] a) J. Zhu, S. Wei, X. Chen, A. B. Karki, D. Rutman, D. P. Young, Z. Guo, *J. Phys. Chem. C* **2010**, *114*, 8844; b) J. Zhu, S. Wei, Y. Li, L. Sun, N. Haldolaarachchige, D. P. Young, C. Southworth, A. Khasanov, Z. Luo, Z. Guo, *Macromolecules* **2011**, *44*, 4382.
[15] A. Funck, W. Kaminsky, *Compos. Sci. Technol.* **2007**, *67*, 906.
[16] K. Wakabayashi, P. J. Brunner, J. I. Masuda, S. A. Hewlett, J. M. Torkelson, *Polymer* **2010**, *51*, 5525.
[17] a) X. Chen, S. Wei, A. Yadav, R. Patil, J. Zhu, R. Ximenes, L. Sun, Z. Guo, *Macromol. Mater. Eng.* **2011**, *296*, 434; b) S. Wei, R. Patil, L. Sun, N. Haldolaarachchige, X. Chen, D. P. Young, Z. Guo, *Macromol. Mater. Eng.* **2011**, DOI: 10.1002/mame.201100010.
[18] M. Xiao, L. Sun, J. Liu, Y. Li, K. Gong, *Polymer* **2002**, *43*, 2245.
[19] L. Sun, J. Y. O'Reilly, C.-W. Tien, H.-J. Sue, *J. Chem. Educ.* **2008**, *85*, 1105.
[20] G. Chen, X. Chen, H. Wang, D. J. Wu, *Appl. Polym. Sci.* **2007**, *103*, 3470.
[21] G. Sui, W. H. Zhong, X. Ren, X. Q. Wang, X. P. Yang, *Mater. Chem. Phys.* **2009**, *115*, 404.
[22] H. Kim, S. Kobayashi, M. A. AbdurRahim, M. J. Zhang, A. Khusainova, M. A. Hillmyer, A. A. Abdala, C. W. Macosko, *Polymer* **2011**, *52*, 1837.
[23] F. Du, R. C. Scogna, W. Zhou, S. Brand, J. E. Fischer, K. I. Winey, *Macromolecules* **2004**, *37*, 9048.
[24] G. Chen, C. Wu, W. Weng, D. Wu, W. Yan, *Polymer* **2003**, *44*, 1781.
[25] N. Grossiord, M. E. L. Wouters, H. E. Miltner, K. Lu, J. Loos, B. V. Mele, C. E. Koning, *Eur. Polym. J.* **2010**, *46*, 1833.
[26] L. Sun, J. Liu, S. R. Kirumakki, E. D. Schwerdtfeger, R. J. Howell, K. Al-Bahily, S. A. Miller, A. Clearfield, H.-J. Sue, *Chem. Mater.* **2009**, *21*, 1154.
[27] F. M. Uhl, C. A. Wilkie, *Polym. Degrad. Stab.* **2002**, *76*, 111.
[28] M. Yoonessi, J. R. Gaier, *ACS Nano* **2010**, *4*, 7211.
[29] R. Santhanam, P. Kamaraj, M. Noel, *J. Power Sources* **1998**, *72*, 239.
[30] D. N. Busick, R. J. Spontak, C. M. Balik, *Polymer* **1999**, *40*, 6023.
[31] *Polymer Nanocomposites*, (Eds., Y.-W. Mai, Z.-Z. Yu), Woodhead Publishing, Cambridge **2006**.
[32] J. A. King, B. A. Johnson, M. D. Via, C. J. Ciarkowski, *J. Appl. Polym. Sci.* **2009**, *112*, 425.
[33] J. A. King, M. D. Via, J. M. Keith, F. A. Morrison, *J. Compos. Mater.* **2009**, *43*, 3073.
[34] R. Dweiri, J. Sahari, *J. Power Sources* **2007**, *171*, 424.
[35] G. Chen, D. Wu, W. Weng, C. Wu, *Carbon* **2003**, *41*, 619.
[36] H. Fukushima, L. Drzal, B. Rook, M. Rich, *J. Therm. Anal. Calorim.* **2006**, *85*, 235.
[37] E. T. Thostenson, C. Li, T.-W. Chou, *Compos. Sci. Technol.* **2005**, *65*, 491.
[38] S. Stankovich, D. A. Dikin, G. H. B. Dommett, K. M. Kohlhaas, E. J. Zimney, E. A. Stach, R. D. Piner, S. T. Nguyen, R. S. Ruoff, *Nature* **2006**, *442*, 282.
[39] G. Chen, W. Zhao, in *Nano- and Biocomposites*, (Eds., A. K.-T. Lau, F. Hussain, K. Lafdi), CRC Press, Boca Raton **2010**.
[40] P. Morgan, *Carbon Fiber and Their Composites*, Taylor & Francis, Boca Raton **2005**.
[41] A. Chatterjee, B. L. Deopura, *J. Appl. Polym. Sci.* **2006**, *100*, 3574.
[42] T. V. Monakhova, P. M. Nedorezova, T. A. Bogayevskaya, V. I. Tsvetkova, Y. A. Shlyapnikov, *Polym. Sci. USSR* **1988**, *30*, 2589.
[43] H. Kim, C. W. Macosko, *Macromolecules* **2008**, *41*, 3317.
[44] R. Kotsilkava, in *Thermoset Nanocomposites for Engineering Applications* (Ed., R. Kotsilkava), Smithers Rapra Technology Limited, Shropshire, UK **2007**.
[45] L. Chen, L. Lu, D. Wu, G. Chen, *Polym. Compos.* **2007**, *28*, 493.
[46] T. Nishino, T. Matsumoto, K. Nakamae, *Polym. Eng. Sci.* **2000**, *40*, 336.
[47] G. Machado, E. L. G. Denardin, E. J. Kinast, M. C. Gonçalves, M. A. de Luca, S. R. Teixeira, D. Samios, *Eur. Polym. J.* **2005**, *41*, 129.
[48] J. W. Anthony, R. A. Bideaux, K. W. Bladh, M. C. Nichols, *Handbook of Mineralogy*, Mineral Data Publishing, The Mineralogical Society of America, Tucson Arizona, USA **1990**.
[49] J. Fayos, *J. Solid State Chem.* **1999**, *148*, 278.
[50] Z. Q. Li, C. J. Lu, Z. P. Xia, Y. Zhou, Z. Luo, *Carbon* **2007**, *45*, 1686.
[51] Q. Yuan, R. D. K. Misra, *Polymer* **2006**, *47*, 4421.
[52] J. M. Keith, J. A. King, B. A. Johnson, *J. New Mater. Electrochem. Syst.* **2008**, *11*, 253.
[53] P. Barber, S. Balasubramanian, Y. Anguchamy, S. Gong, A. Wibowo, H. Gao, H. Ploehn, H.-C. Zur Loye, *Materials* **2009**, *2*, 1697.
[54] H. Nalwa, *Handbook of Low and High Dielectric Constant Materials and Their Applications*, Academic Press, London, UK **1999**.
[55] T. Osaka, M. Datta, *Energy Storage Systems for Electronics*, Gordon and Breach, Amsterdam, The Netherlands **2001**.
[56] J. Bird, *Electrical Circuit Theory and Technology*, 3rd edition, *Newnes* **2007**.
[57] J. D. Ferry, *Viscoelastic Properties of Polymers*, 3rd edition, Wiley, New York **1980**.
[58] M. Sugimoto, T. Tanaka, Y. Masubuchi, J. I. Takimoto, K. Koyama, *J. Appl. Polym. Sci.* **1999**, *73*, 1493.